Tapered channel for six-dimensional muon cooling towards micron-scale emittances

Diktys Stratakis, Richard C. Fernow, J. Scott Berg, and Robert B. Palmer
Brookhaven National Laboratory, Upton, New York 11973, USA
(Received 19 June 2013; published 23 September 2013)

A high-luminosity muon collider requires a significant reduction of the six-dimensional emittance prior to acceleration. Obtaining the desired final emittances requires transporting the muon beam through long sections of a beam channel containing rf cavities, absorbers, and focusing solenoids. Here we propose a new scheme to improve the performance of the channel, consequently increasing the number of transmitted muons and the lattice cooling efficiency. The key idea of our scheme is to tune progressively the main lattice parameters, such as the cell dimensions, rf frequency, and coil strengths, while always keeping the beam emittance significantly above the equilibrium value. We adopt this approach for a new cooling lattice design for a muon collider, and examine its performance numerically. We show that with tapering the cooling rate is not only higher than conventional designs, but also maintains its performance through the channel, resulting in a notable 6D emittance decrease by 3 orders of magnitude. We also review important lattice parameters, such as the required focusing fields, absorber length, cavity frequency, and voltage.

DOI: 10.1103/PhysRevSTAB.16.091001 PACS numbers: 29.20.Ej, 41.75.Lx

I. INTRODUCTION

Muon colliders allow the high-energy study of pointlike collisions of leptons without some of the difficulties associated with electrons, such as the synchrotron radiation that requires their acceleration to be essentially linear and, for this reason, long and costly [1]. A key technical challenge in the development of a muon collider is that the phase space of the beam that comes from pion decay greatly exceeds the acceptance of downstream accelerator systems and therefore, a cooling channel is required. In addition, reducing the beam emittance is an essential step for achieving high luminosity in a muon collider. Given the short lifetime of a muon particle, ionization cooling is the only practical method that can be realized [2].

In ionization cooling, the beam loses both transverse and longitudinal momentum as it passes through a material medium. Subsequently, the longitudinal momentum can be restored by reacceleration, leaving a net loss of transverse momentum. Only the transverse phase space becomes smaller by this process. This may be enough for accelerator applications such a neutrino factory [3], however for a muon collider [4] or a Higgs factory [5] cooling of the longitudinal emittance is needed as well.

Over the past decade much progress has been made in the design and simulation of 6D cooling lattices [6–12] based on emittance exchange. This is generally accomplished by using a wedge-shaped absorber or a differential path length in a region with nonzero dispersion. Particles with higher energies pass through more material than particles with lower energy as a result of dispersion, eventually leading to reduction of both longitudinal and transverse emittance. In particular, ring-shaped coolers that use tilted solenoids to generate dispersion have been shown to provide an impressive 2 orders of magnitude reduction of the normalized 6D phase-space volume with a transmission above 50% [6]. This design later evolved into a helical channel referred to as a ''Guggenheim'' in order to avoid serious problems with injection and extraction of large emittance beams [11]. It was found that the performance of a Guggenheim lattice is comparable to the original cooler ring [13].

It is important to emphasize that the previously designed cooling lattices used a constant radius of curvature, thus reducing the available dispersion for emittance exchange. Furthermore, they had fixed focusing along the channel, causing a reduction in cooling rate as the emittance approached its equilibrium value. Hence, it is likely that the cooling performance of the channel will be limited by the lattice parameters, and it is uncertain whether we can achieve the micron-scale emittances required for a muon collider [1]. For this reason it is important to examine new designs that improve the lattice performance by minimizing possible cooling limitations.

It has been suggested [14] that the lattice performance can be enhanced by using a tapered scheme in which parameters of the structure, such as the cell length, focusing, and radius of curvature, change from to turn to turn, so that the beam emittance is always larger than the equilibrium emittance. Computations have shown that with this configuration the dispersion required to produce emittance exchange can be increased up to a factor of 2 [15], while

the required length for cooling can be reduced substantially compared to a conventional lattice [16].

In this paper we present results of our simulation extending the concept of tapering to 6D ionization cooling channels for a muon collider. We show that with tapering the cooling rate is not only higher than conventional designs, but also maintains its performance through the channel, resulting in a notable 6D emittance decrease by 3 orders of magnitude. Our findings indicate that even with inclusion of reasonable safety factors, the needed fields are consistent with the critical limits of existing conductor technology while the maximum field on the coil is less by 15% compared to previous estimates [17]. With the aid of this work the rf frequencies, rf gradients, and magnetic fields can now be specified to a level that a first order cost and practicality study can be implemented. For instance, we show that a small number of different frequencies, namely 201, 402, 603 and 805 MHz, are enough to cool towards the baseline cooling requirements.

The outline of this paper is as follows: In Sec. II, we give an overview of the ionization cooling concept. In Sec. III, we provide details of the design parameters for the proposed cooling channel. In Sec. IV we report the results from our simulations modeling of the aforementioned channel. Finally, we present our conclusions in Sec. V.

II. IONIZATION COOLING

Ionization cooling involves passing the beam through material in which the muons lose both transverse and longitudinal momentum by ionization energy loss, commonly referred to as dE/dx. The longitudinal momentum can be restored by reacceleration, leaving a net loss of transverse momentum. The equation describing the rate of cooling is a balance between cooling (first term) and heating (second term) effects [18,19]:

$$\frac{d\varepsilon_n}{ds} = -\frac{1}{\beta^2}\frac{dE_\mu}{ds}\frac{\varepsilon_n}{E_\mu} + \frac{1}{\beta^3}\frac{\beta_T(E_s)^2}{2E_\mu m_\mu c^2 L_R}, \qquad (1)$$

where ε_n is the normalized transverse emittance, E_μ is the muon energy in GeV, m_μ is the muon mass, β_T is the transverse betatron function within a discrete absorber, β is the particle velocity, c is the speed of light, dE_μ/ds is the energy loss per unit length, L_R is the radiation length of the material, and E_s is the characteristic scattering energy ($\sim$13.6 MeV).

The minimum normalized transverse emittance that can be achieved for a given absorber in a given focusing field is reached when the cooling rate equals the heating rate in Eq. (1):

$$\varepsilon_{N,\mathrm{min}} = \frac{\beta_T(E_s)^2}{2\beta m_\mu c^2 L_R |\frac{dE_\mu}{ds}|}. \qquad (2)$$

For a muon collider, it is desirable to reduce the longitudinal emittance as well. There is a well-known method for accomplishing this, often referred to as "emittance exchange." This can be implemented by using a wedge-shaped absorber in a region with nonzero dispersion. As a result of dispersion, particles with higher energy will pass through more material than particles with lower energy and therefore the energy spread in the beam will be reduced. However, in this process the beam horizontal emittance is increased. The process is thus primarily an exchange of emittance between the longitudinal and transverse dimensions, but when combined with transverse cooling in the material, all three dimensions can be cooled.

Transverse ionization cooling can take place in principle at any momentum. However, at low momentum the slope of the dE/dx curve causes lower momentum particles to lose more energy than higher energy particles. This increases the energy spread and leads to a blowup in the longitudinal emittance. Cooling at high momentum is uneconomical since a lot of rf power is required to replace a fixed fraction of the initial energy. For these reasons cooling channels are typically designed [20] with a reference momentum near the minimum of the dE/dx curve ($\approx$200 MeV/c). The momentum is sometimes reduced in the final stages of the channel in order to reduce the value of the beta function and to take advantage of the higher value of dE/dx.

Typical 6D cooling requirements for a muon collider demand a reduction of the normalized transverse emittance by almost 3 orders of magnitude and a reduction of the longitudinal emittance by more than an order of magnitude [1]. This cooling is achieved in a series of cooling cells. Each cell consists of solenoids for focusing, weak dipoles to generate bending and dispersion, wedge-shaped absorbers where cooling takes place, and rf cavities to replenish the energy lost in the absorbers.

We note that there are several engineering constraints on any practical magnetic configuration and some of those will be addressed in the next section. The operating current in a superconducting magnet must be smaller than the critical current corresponding to the peak field in the coil, the arrangement of the coils must allow access to the rf cavities and absorbers, and there may be constraints on the strength and direction of the magnetic field in the rf cavities to prevent breakdown from limiting the useful electric field gradient in the cavity [21].

III. 6D COOLING LATTICES FOR MUON COLLIDERS

A complete scheme for cooling a muon beam sufficiently for use in a muon collider has been previously described [1]. This scheme uses separate 6D ionization cooling channels for the two signs of the particle charge. In each, a channel first reduces the emittance of a train of muon bunches until they can be injected into a bunch-merging system. The single muon bunches, one of each sign, are then sent through a second 6D cooling channel

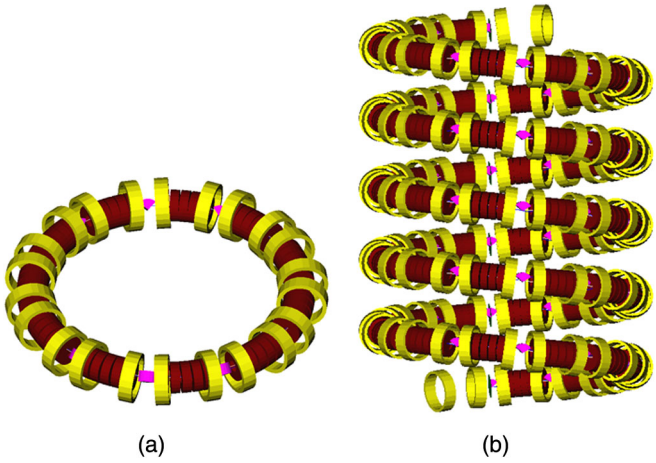

FIG. 1. (a) Drawing of an idealized RFOFO cooling ring; (b) 5 turn slice of a Guggenheim helix. The large yellow cylinders are solenoids, the small red cylinders are the active volume of the rf cavities, and the magenta wedges are hydrogen absorbers.

where the transverse emittance is reduced as much as possible and the longitudinal emittance is cooled to a value below that needed for the collider. The beam can then be recombined and sent though a final cooling channel using high-field solenoids that cools the transverse emittance to the required value of the collider while allowing the longitudinal emittance to grow. Most studies [6] so far have been focused on the regime before the bunch-merging system where only a modest transverse cooling to $\sim$1.3 mm is required, while very little is known for the post-bunch-merging regime where a final $<$0.3 mm rms normalized emittance is desired. This paper focuses on the design and simulation of a 6D cooling channel for a single muon bunch after it exits the bunch merger system.

The idea for the 6D cooling channel described here originated from the conventional reverse focus focus (RFOFO) cooling ring in Ref. [6]. Historically, the FOFO part of the name refers to the focusing-drift focusing nature of the solenoid lattice, in analogy to the FODO lattice for quadrupole channels. The conventional ring design employs a single cell for both transverse cooling and emittance exchange. It uses solenoids for focusing, giving large angular and momentum acceptances. The cell includes dispersion, acceleration, and energy loss in a single thick liquid hydrogen wedge. The overall layout of the ring is shown in Fig. 1(a).

The ring consists of 12 identical cells with two or four solenoids in each cell with opposite polarity to provide transverse focusing. The coils (yellow) are not evenly spaced; those on either side of the absorber are closer together in order to increase the focusing at the wedge absorber (magenta) and thus minimizing the beta function at that location. The relative amount of cooling can be adjusted by changing the opening angle and transverse location of the wedge. A series of rf cavities (dark red) are used to restore the momentum along the longitudinal axis. The dispersion necessary for emittance exchange is provided from the bend field generated by tilting the axes of the solenoids above and below the orbital midplane [Fig. 2(a)]. The RFOFO ring design evolved into a helical channel [see Fig. 1(b)] commonly referred to as a Guggenheim in order to avoid serious problems with injection of large emittance beams. This lattice inherits most of the parameters of the ring with little or no change and the only difference is the change of elevation of the elements [11].

The main disadvantage of the lattices shown in Fig. 1 is that they used a fixed set of parameters for the radius of curvature, cell length, rf frequency, amount of the absorbing material and magnetic field strength, consequently opposing any cooling beyond the equilibrium emittance. To further improve the performance of the cooling lattice, we propose here a tapered channel in which the aforementioned parameters change gradually with distance. At the

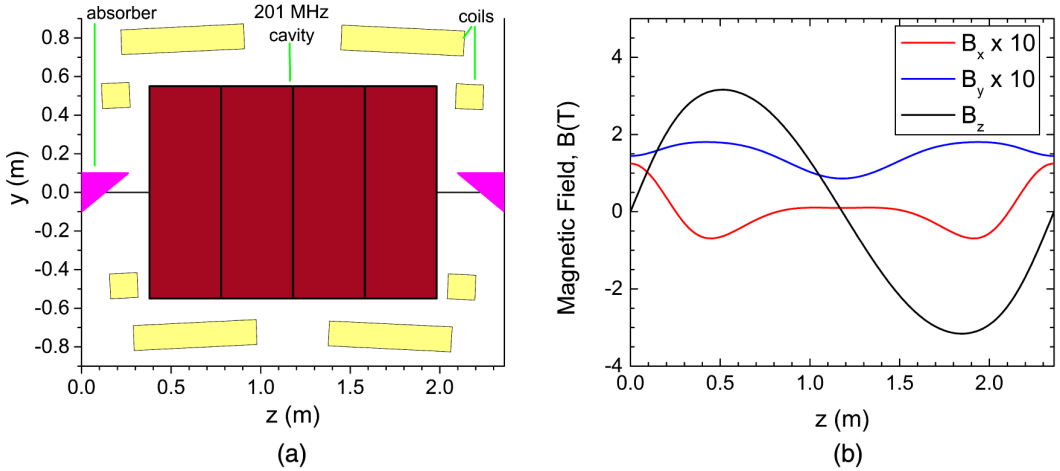

FIG. 2. (a) Side view of one cell for stage 2; (b) magnetic field on axis along the cell. The horizontal field B_x is shown in red, the vertical field B_y is shown in blue, and the longitudinal field B_z is shown in black.

TABLE I. Main lattice parameters of a tapered ziggurat shaped helical lattice.

Stage	Cell length [m]	Cell number	Pipe radius [cm]	rf frequency [MHz]	rf volume [MV/m]	rf number	Coil displacement [cm]	Coil tilt [deg]	Wedge angle [deg]	Momentum acceptance [MeV/c]
1	2.75	11	21.5	201	16.5	5	12.5	3.25	98	91
2	2.36	16	18.7	201	16.5	4	10.3	2.59	100	94
3	2.02	16	16.2	201	16.5	4	10.3	2.03	110	92
4	1.73	15	14.1	402	16.5	6	5.3	3.90	99	92
5	1.49	18	11.8	402	16.5	5	6.4	2.62	104	91
6	1.38	26	10.2	402	17.5	5	6.4	2.62	111.3	90
7	1.27	24	9.1	402	17.5	6	6.4	1.91	118	85
8	1.15	19	7.3	402	17.5	5	6.4	1.93	120	84
9	0.995	29	6.7	603	19.5	5	4.1	2.46	120	83
10	0.806	46	6.0	603	20.5	5	2.6	2.46	110	82
11	0.688	42	5.5	805	23.5	4	1.9	2.79	120	79
12	0.688	54	5.0	805	23.5	4	1.5	2.95	120	77
13	0.688	46	4.5	805	23.6	4	1.4	3.28	120	72
14	0.628	43	4.0	805	23.6	4	1.2	2.87	120	68
15	0.608	39	3.5	805	23.6	4	1.1	2.89	120	66
16	0.588	28	3.1	805	23.6	4	0.9	2.97	120	64
17	0.588	20	2.8	805	23.4	4	0.9	2.81	116	67

first stage of the tapered channel the focusing will be relatively weak to avoid excessive angular divergence that can arise from the large transverse emittance of the initial muon beam. However, the weak focusing implies that the beta function and thus the equilibrium emittance are also relatively large, so the transverse cooling weakens as the limit is approached. To avoid this, this stage is terminated and we couple into the next stage that has a lower beta. This is achieved by simultaneously scaling down the cell dimensions and raising the strength of the on-axis solenoidal field. As a result this will produce a piecewise constant multistage "ziggurat" shaped channel [22] where each stage will be a fixed-radius helical channel consisting of a series of identical cells similar to the one shown in Fig. 1(b). Here it is interesting to recall that a comparison between a tapered and untapered channel [16] revealed that tapering reduces the length of the cooling channel substantially and achieves a lower 6D cooling emittance at the same time. As we will demonstrate in Sec. IV, 17 tapered stages are enough to cool towards the baseline requirements of a muon collider. The required lattice parameters are summarized in more detail in Table I.

Figure 2(a) shows the side view of one cell at an early stage of the channel (stage 2). This stage consists of a sequence of 12 identical 2.36 m cells, each containing four 0.4 m-long 201 MHz pillbox cavities, and a wedge-shaped liquid hydrogen absorber, with 28.6 cm central thickness and 100 deg opening angle, to assure energy loss. Moreover, each cell contains four solenoid coils of opposite polarity, yielding an approximate sinusoidal variation of the magnetic field in the channel with a peak on-axis value of 3.11 T and providing transverse focusing with a peak beta value of ~37 cm. The tilt of solenoids is adjusted to provide a mean bending field of 0.148 T in order to provide adequate emittance exchange. In order to minimize the integrated on-axis radial field, which can cause vertical beam deviations, the centers of the solenoids are slightly displaced radially outward from the beam axis. The peak accelerating gradient of the rf cavities is 16.5 MV/m, while each operates at a synchronous phase 34 deg off the 0-crossing point. The irises of the pillbox cavities are enclosed with 150 μm beryllium (Be) windows. The Be windows roughly double the cavity shunt impedance, and give a higher field on axis for a given amount of rf power [23].

Figure 3 illustrates some basic lattice properties of stage 2. Notice from Fig. 3(a) that the lattice transmits in a wide momentum band, namely from 155 to 248 MeV/c, with a central momentum of 205 MeV/c. Figure 3(b) displays the beta as a function of position along the cell at the central momentum. One can see that the absorber is positioned at a position where the transverse beta becomes minimum. Since the lattice equilibrium emittance is proportional to the beta function, placing the absorber on that location would enhance (at least in theory) the cooling rate compared to any other location in the cell. Deviation of the closed orbit along the cell for various momenta ranging from 185 to 225 MeV/c in 10 MeV/c increments is shown in Fig. 3(c). Notice that at the central momentum the vertical offset (blue) and horizontal offset (red) from the center is near zero at the entrance of the cell. This implies that no off-axis displacements of the absorber wedges are necessary consequently simplifying the structure layout. Figure 3(d) displays the dispersion functions in

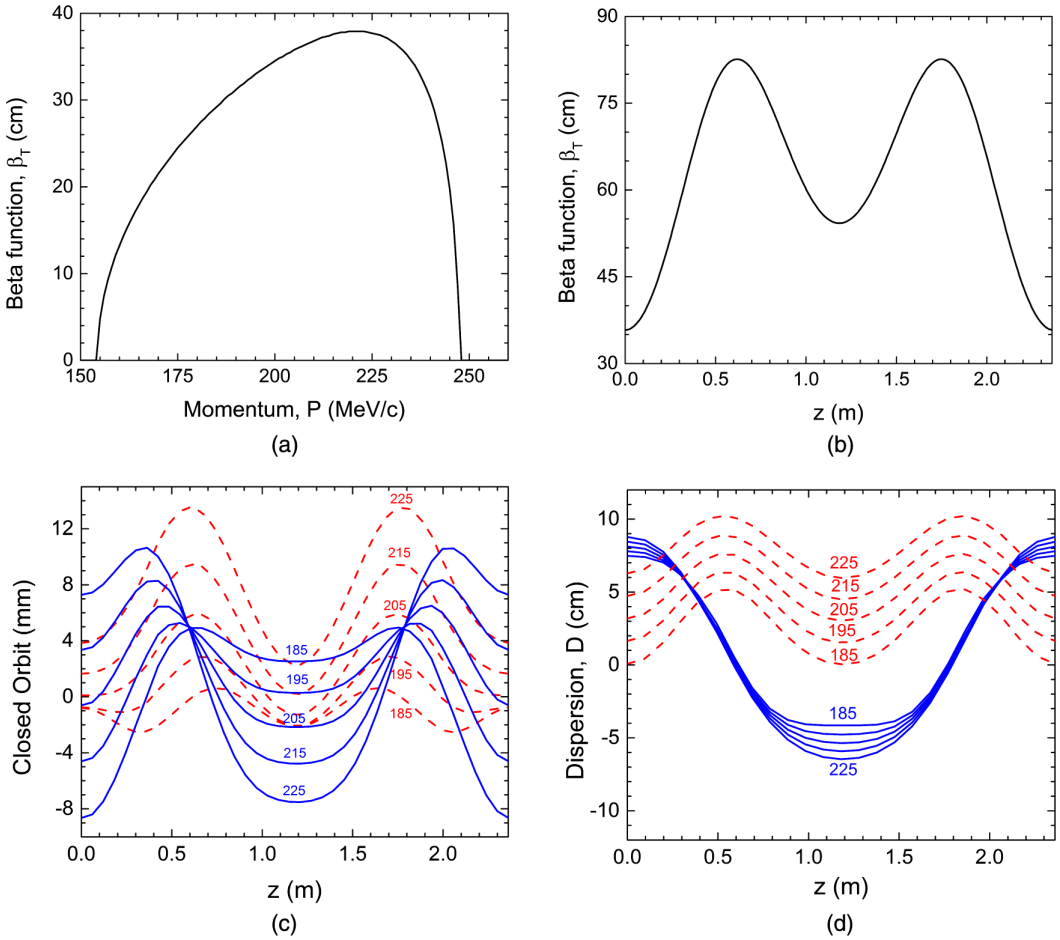

FIG. 3. Lattice properties for stage 2. (a) Beta function at the absorber center vs momentum; (b) beta function vs position at the reference momentum of 205 Mev/c; (c) deviations from the central line of the channel in the horizontal direction (red) and in the vertical direction (blue). The different lines correspond to orbits of different momentum muons; (d) dispersion vs position for different momentum muons.

x (red) and y (blue) at the absorber central plane. The dispersion at the absorber has the same sign in both directions and is mostly in the y direction. While the horizontal dispersion is increasing progressively with energy, the vertical is not.

Figure 4(a) shows a cell for a later stage (stage 11) that is appropriate to cool to <0.6 mm normalized rms transverse emittances. To achieve this we design a lattice cell with a considerably smaller betatron function and thus equilibrium emittance. Therefore, we place the coils closer to the axis and reduce the lattice period, L, to 0.688 m ($\beta_T \propto L$). Moreover, we scale up the magnetic field to increase the muon focusing at the absorber. Stage 11 consists of 34 identical cells, each containing four 8.59 cm-long 805 MHz pillbox cavities and wedge-shaped liquid hydrogen absorbers to produce the energy loss as before. Figure 4(b) displays the on-axis horizontal, vertical and longitudinal (axial) fields along the cell. As in stage 2, the longitudinal magnetic field has an approximately sinusoidal dependence on position. The peak magnitude is 11.7 T on axis and 14.5 T in the coil. The solenoids are tilted by 2.79 deg to generate a mean bending field of 0.51 T. Notice that the bending field is significantly more than the field of 0.148 T required at stage 2.

Figure 5(a) shows the dependence of the transverse beta function on the muon momentum at the center of the absorber. It demonstrates that the lattice transmits particles in the momentum band 165–242 MeV/c with a central momentum of 195 MeV/c. Figure 5(b) illustrates the beta function at the reference (central) momentum as a function of the axial position in the cell. It is interesting to note that near the reference momentum the closed orbits remain in close proximity to the axis [Fig. 5(c)], while the dispersion at the absorbers is primarily in the vertical direction [Fig. 5 (d)]. As desired, the dispersion is maximum at the location of the absorber ensuring adequate emittance exchange. By carefully examining Figs. 2 and 4 the following points are noteworthy: First, the dispersion at the cell entrance of stage 11 is 3 times smaller than in stage 2, which is a direct consequence of the almost 3 times stronger axial

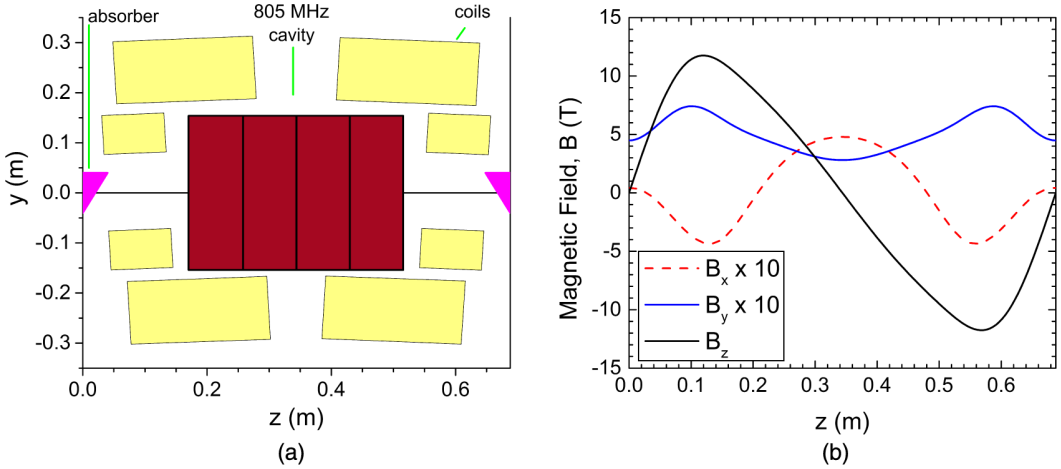

FIG. 4. (a) Side view of one cell for stage 11; (b) magnetic field on axis along the cell. The horizontal field B_x is shown in red, the vertical field B_y is shown in blue, and the longitudinal field B_z is shown in black.

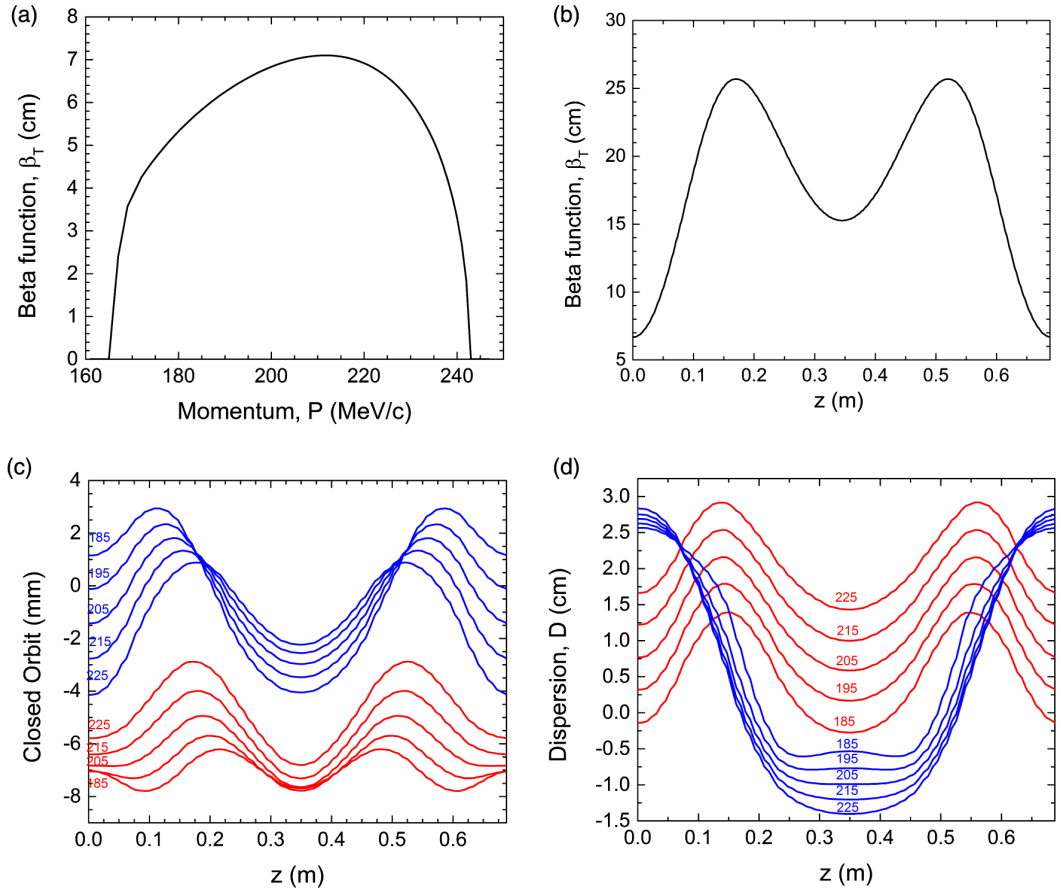

FIG. 5. Lattice properties for stage 11. (a) Beta function at the absorber center vs momentum; (b) beta function vs position at the reference momentum of 195 MeV/c; (c) deviations from the central line of the channel in the horizontal direction (red) and in the vertical direction (blue). The different lines correspond to orbits of different momentum muons; (d) dispersion vs position for different momentum muons.

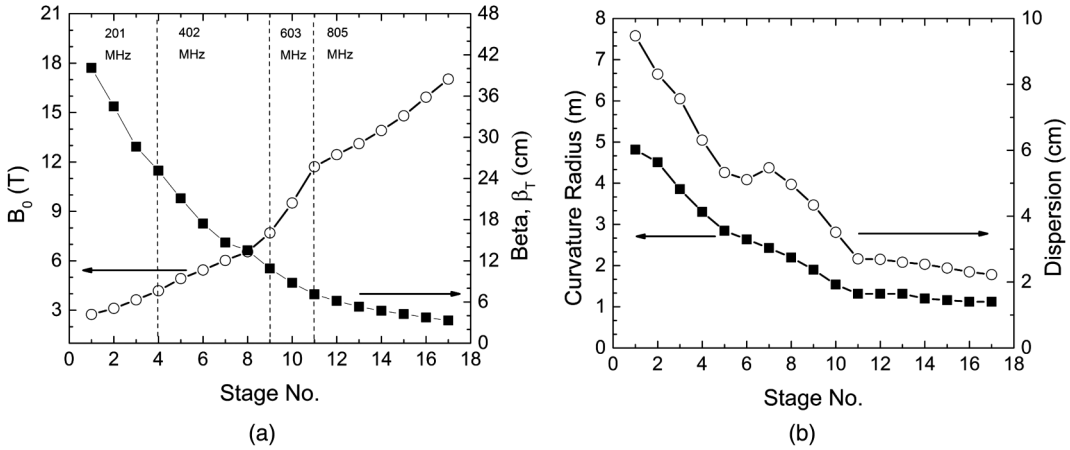

FIG. 6. (a) Design value of beta function (right) and maximum value of the on-axis solenoid field; (b) radius of curvature and dispersions at various stages of our ziggurat channel.

magnetic field. Here it is interesting to recall that this dispersion is still 2 times higher than that of the equivalent stage of an untapered Guggenheim channel [15]. Moreover, the transverse beta function for stage 11 is $\beta_T <$ 8 cm, which is required as the normalized rms emittance must be reduced $<$0.6 mm as the beam exits the stage. However, to achieve this, we need to scale up the magnetic field to increase the muon focusing at the absorber. A technical challenge may arise as the operating current on the conductor should not exceed the critical current corresponding to the peak field in the coil. The implication of this will be discussed in more detail in the next section.

Figure 6(a) exhibits the beta function and the axial peak field at different stages. The beta function varies from 40.1 to 3.3 cm, while the on-axis magnetic field increases from 2.7 to 17.0 T. The last column of Table I indicates the momentum acceptance of each stage. Similar to Ref. [20], the momentum acceptance is reduced as the beta function becomes smaller and smaller. For instance, while the momentum acceptance is above 90 MeV/c at the first stages, it drops below 70 MeV/c for the last four stages. Figure 6(b) displays the radius of curvature and dispersion at the absorber center for various stages. We found that using a constant radius of curvature did not produce adequate dispersion to give the required longitudinal cooling. As a result, we adjusted the radius of curvature of each stage to be proportional to the changes of the beta function. Quantitatively, by using this configuration the dispersion increased up to a factor of 2 [15]. Ideally, the cooling channel should be tapered with various parameters changing very slowly along the channel. However, this can lead to feasibility and cost challenges. For instance, changing the rf frequency continuously is very expensive, so the number of different frequencies for tapering should be as small as possible. In our lattice we choose only four different rf frequencies, namely 201, 402, 603, and 805 MHz. As we will demonstrate shortly, this arrangement is sufficient to achieve the desired cooling emittance for a muon collider.

IV. TRACKING STUDIES

The performance of the cooling channel was simulated using the ICOOL code [24]. The code includes all relevant physical processes (e.g. energy loss, straggling, multiple scattering) and includes muon decay. For each stage, we generated 3D cylindrical field maps by superimposing the fields from all solenoids in the cell and its neighbor cells. The resultant field components were shown to satisfy the 3D Maxwell equations to a high level of accuracy and agreed with independent calculations [25]. The rf cavities were modeled using cylindrical pillboxes running in the TM010 mode and a reference particle was used to determine each cavity's relative phase. Both irises were covered by a thin beryllium window in order to produce the maximum electric field on axis for a given amount of rf power. The window thickness was progressively decreasing from 100 μm (stage 1) to 10 μm (stage 17) and for all stages its diameter was equal to the pipe aperture. The aperture was also gradually decreasing along the channel (see Table I) in order to accommodate the higher frequency rf cavities for the later stages. The absorber material was liquid hydrogen and it was enclosed in AlBeMet (beryllium-aluminum composite material) safety windows ranging in thickness from 500 μm (stage 1) to 10 μm (stage 17). For simplicity, we assumed that the windows are planar and located axially on both sides of the wedge but in reality the window shape needs to conform to the absorber.

The input beam in the simulations has a normalized transverse emittance of 3.63 mm and a normalized longitudinal emittance of 10.17 mm, while the average longitudinal momentum is 218 MeV/c. Those parameters closely resemble the baseline distribution of a muon beam before the final 6D cooling sequence of a muon collider [1]. We tracked 100 000 particles and included decay of muons.

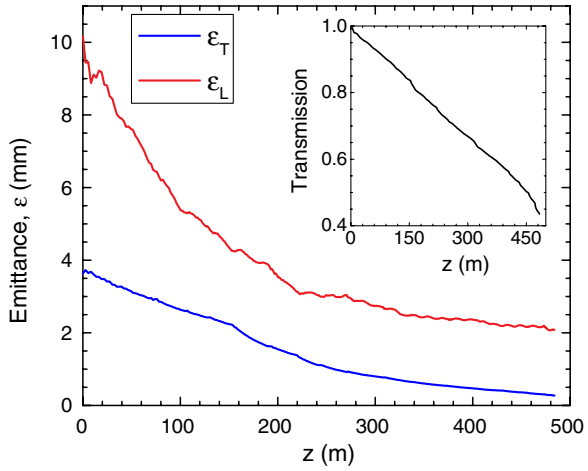

FIG. 7. Simulation results of the performance of a tapered 6D cooling channel for a muon collider. The plot shows the evolution of the normalized rms emittances and transmissions as a function of distance along the channel. At $z = 480$ m the transmission is 45% with muon decays, while the final emittances are $\varepsilon_T = 0.27$ mm and $\varepsilon_L = 2.0$ mm.

Note that average momentum does not remain constant along the channel but is reduced by ~10–15 MeV/c in the final seven stages in order to reduce the value of the transverse beta function. This is because in a solenoidal channel, the beta function is proportional to the momentum and inversely proportional to the axial field. Therefore, for a given strength magnet we can focus the beam stronger if we lower the momentum.

The transverse and longitudinal emittances and the transmission are shown as a function of distance along the channel in Fig. 7. It is worth noting that after a distance of 480 m (17 stages) the 6D emittance has fallen by a factor of 1000 with a transmission of 45%. In addition, at the end of the channel the transverse emittance decreased by a factor of ~14, while the longitudinal emittance shrank by a factor of ~5. By carefully examining the results in Fig. 7, the following points are noteworthy. First, earlier simulations [26] revealed severe particle loss and emittance growth due to space charge if the longitudinal emittance approaches the limit of 1.5 mm. Thus, to assure satisfactory cooling with minimum losses we choose to cool longitudinally only down to 2 mm. Second, and most importantly, a transverse emittance $\varepsilon_T < 300$ μm is the baseline requirement for a muon collider after the final 6D cooling sequence. We can conclude from the results in Fig. 7 that 17 stages are enough to fulfill this requirement since the simulation produced a final transverse emittance of 270 μm.

The cooling efficiency [6] of the lattice is often characterized in terms of the quality factor,

$$Q = \frac{d\epsilon_{6D}^N/ds}{dN/ds}\frac{N(s)}{\epsilon_{6D}^N}, \tag{3}$$

where ϵ_{6D}^N is the normalized six-dimensional emittance of the beam and $N(s)$ is the number of surviving particles at arclength s. The Q factor compares the rate of change of emittance to the particle loss and under ideal conditions should remain the same (constant) through the lattice. In conventional lattices Q starts off small due to losses from initial mismatching, then rises to a large value and finally falls as the emittance of the beam approaches its equilibrium value. Figure 8 shows the evolution of Q along the channel. A glance at Fig. 8 indicates the importance of tapering as the cooling rate remains relatively flat and drops only by 15% at 480 m relative to its maximum value ($Q \approx 11$). It is worth noting that repeating the same simulation with an untapered channel we also see a rise in Q. However, its peak value is less ($Q \approx 8$) and drops within 150 m to 2.5 indicating a dramatic decline in cooling efficiency [27].

Figure 9 shows the current densities vs the maximum local fields in the coils used. For these estimates we have used published [28] "engineering" current densities, multiplied by factors to allow for the required support structure, the need for stabilizing copper, and the filling factor for a real conductor. We estimate [29] this factor to be approximately 25% for NbTi and Nb_3Sn cable and 50% for yttrium barium copper oxide (YBCO) tape when used for flip-field designs where the fields are approximately perpendicular with the tape surfaces. The red line illustrates the current density of the coil at the peak field location for each cooling stage. Note from Fig. 9 that there is a relatively rapid increase of the magnet operating current with stage number. This is a direct consequence of the low β_T lattice design which is needed to cool towards micron-scale emittances. At the last stage, the maximum field on the coil is 18 T which is less by 15% compared to previous estimates [17]. In addition, our findings indicate that even with

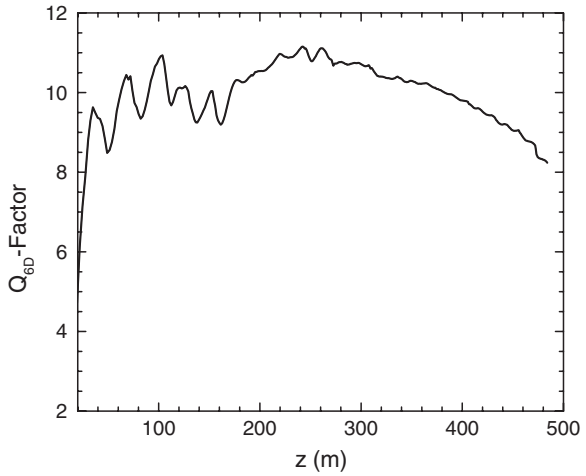

FIG. 8. Evolution of the cooling performance in a tapered cooling lattice. Note that the cooling efficiency Q remains relatively flat through most of the channel, indicating a robust performance, while it drops by only 15% at the last 100 m.

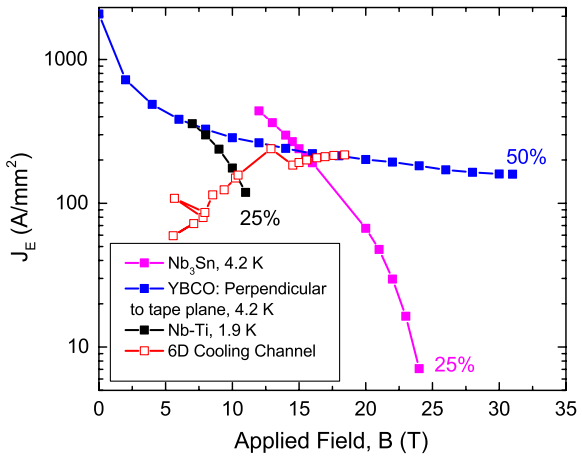

FIG. 9. Engineering critical current densities vs applied magnetic fields for various conductors from published data [28]. The red line plots the required fields and current densities of a tapered muon cooling channel. Note that the current densities of the proposed channel are within the critical limits.

inclusion of reasonable safety factors, the needed fields are consistent with the critical limits of existing conductor technology [28]. However, the last four stages are barely within the limits of YBCO and therefore it is critically important to the development of a muon collider that a well thought-out test program to be continued. Here it is interesting to recall that Gupta *et al.* [30,31] built and tested a 25 mm aperture HTS insert generating >16 T peak field and a 100 mm aperture high temperature superconductors (HTS) midsert generating >9 T peak field. Furthermore, the design and fabrication of a 32 T, 32 mm bore superconducting magnet with high-field REBCO inner coils is underway at the National High Magnetic Field Laboratory [32]. Those efforts show the potential of HTS in accomplishing high fields.

V. SUMMARY

For a muon collider the six-dimensional muon beam phase-space volume must be reduced by several orders of magnitude in order to be able to further accelerate it. Ionization cooling is the only feasible option for cooling the beam within the short muon lifetime ($\tau_0 = 2.2\ \mu$s). It was been suggested that the lattice performance can be enhanced by using a tapered scheme in which parameters of the structure, such as the cell length, focusing, and radius of curvature, change progressively with distance, so that the beam emittance is always larger than the equilibrium emittance. Here we have extended the tapering concept specifically to 6D ionization cooling channels. In particular, we incorporated this idea into a new lattice design for the post-bunch-merge 6D cooling lattice of a muon collider. We showed that with tapering the cooling rate is not only higher than conventional designs, but also maintains its performance through the channel, resulting in a notable 6D emittance decrease by 3 orders of magnitude. We showed that relatively modest magnetic fields ($B <$ 17 T, peak on axis) and a small number of different frequencies, namely 201, 402, 603, and 805 MHz, are enough to cool towards the baseline cooling requirements of a muon collider.

The goal of this work was to present the concept of tapering for 6D cooling, explain its basic features, and verify the scheme by numerical simulations. It is important to emphasize that most previous studies have been focused on the pre-bunch-merging regime of a muon collider where only a modest transverse cooling to ~1.3 mm is required, while very little detailed simulation work has been done for the final post-bunch-merging regime where a <0.3 mm rms normalized emittance is desired. Therefore, with the aid of this work the rf fields and magnetic fields can now be specified to a level that a first order cost and practicality study can be implemented. For a future study, it will be interesting to systematically examine the lattice tolerance to errors of various lattice components such as magnet misalignments or powering errors.

ACKNOWLEDGMENTS

The authors are grateful to H. Witte and R. Ryne for useful discussions. This work is supported by the U.S. Department of Energy, Contract No. DE-AC02-98CH10886.

[1] R. B. Palmer, J. S. Berg, R. C. Fernow *et al.*, in *Proceedings of the 2007 Particle Accelerator Conference, Albuquerque, NM* (IEEE, New York, 2007), p. 1222.
[2] D. Neuffer, Part. Accel. **14**, 75 (1983).
[3] M. M. Alsharo'a *et al.*, Phys. Rev. ST Accel. Beams **6**, 081001 (2003).
[4] C. M. Ankenbrandt *et al.*, Phys. Rev. ST Accel. Beams **2**, 081001 (1999).
[5] D. Neuffer, Muon Accelerator Program Document No. 4348 (2012) [http://map-docdb.fnal.gov/].
[6] R. B. Palmer, V. Balbekov, J. S. Berg *et al.*, Phys. Rev. ST Accel. Beams **8**, 061003 (2005).
[7] V. Balbekov, S. Geer, N. Mokhov, R. Raja, and Z. Usubov, in *Proceedings of the 2001 Particle Accelerator Conference, Chicago, IL* (IEEE, New York, 2001), p. 3867.
[8] V. Balbekov, in *Proceedings of the 2003 Particle Accelerator Conference, Portland, OR* (IEEE, New York, 2003), p. 2017.
[9] K. Yonehara, R. P. Johnson, M. Neubauer, and Y. S. Derbenev, in *Proceedings of the 2010 IPAC, Kyoto, Japan* (ICR, Kyoto, 2010), p. 870.
[10] Y. Alexahin, AIP Conf. Proc. **1222**, 313 (2010).
[11] P. Snopok, G. Hanson, and A. Klier, Int. J. Mod. Phys. A **24**, 987 (2009).
[12] A. Klier and G. G. Hanson, Neutrino Factory/ Muon Collider Document 298 (2004).

[13] P. Snopok and G. Hanson, in *Proceedings of PAC 2009, Vancouver, BC, Canada* (IEEE, Piscataway, NJ, 2009), p. 4381.
[14] R. C. Fernow, J. C. Gallardo, R. B. Palmer, and P. L. Lebrun, in Proceedings of the 2001 Particle Accelerator Conference, Chicago, IL (Ref. [7]), p. 3861.
[15] R. B. Palmer and R. C. Fernow, in *Proceedings of the 2011 Particle Accelerator Conference, New York, NY* (IEEE, New York, 2011), p. 106.
[16] P. Snopok, G. Hanson, and R. Palmer, in *Proceedings of the 2011 Particle Accelerator Conference, New York, NY* (Ref. [15]), p. 217.
[17] R. B. Palmer, Muon Accelerator Document No. 4318-v2 (2011)
[18] A. N. Skrinsky and V. V. Parkhomchuk, Sov. J. Part. Nucl. **12**, 223 (1981).
[19] A. W. Chao and M. Tigner, *Handbook of Accelerator Physics and Engineering* (World Scientific, Singapore, 1999).
[20] R. C. Fernow and R. B. Palmer, Phys. Rev. ST Accel. Beams **10**, 064001 (2007).
[21] D. Stratakis, J. C. Gallardo, and R. B. Palmer, Nucl. Instrum. Methods Phys. Res., Sect. A **620**, 147 (2010).
[22] See Fig. 1 in D. Stratakis, R. C. Fernow, and R. B. Palmer, in Proceedings of the 2013 IPAC Conference, Shanghai, China (2013), TUPFI086.
[23] D. Li *et al.*, J. Phys. G **29**, 1683 (2003).
[24] R. C. Fernow, in *Proceedings of the 2005 Particle Accelerator Conference, Knoxville, TN* (IEEE, Piscataway, NJ, 2005), p. 2651.
[25] S. Bracker, Neutrino Factory/ Muon Collider Document 271 (2003).
[26] D. Stratakis, R. B. Palmer, and D. P. Grote, in Proceedings of the 2013 IPAC Conference, Shanghai, China (2013), p. 1553.
[27] R. B. Palmer, Muon Collider Design Workshop (Newport News, VA, 2009) [http://conferences.jlab.org/muon/talks/Palmer.pdf].
[28] http://fs.magnet.fsu.edu/~lee/plot/plot.htm.
[29] R. B. Palmer and H. Kirk (private communication).
[30] R. Gupta *et al.*, IEEE Trans. Appl. Supercond. **21**, 1884 (2011).
[31] R. Gupta *et al.* (unpublished) [http://www.bnl.gov/magnets/staff/gupta/publications/mt23/gupta-mt23-pre-pub.pdf].
[32] W. D. Markiewicz, D. C. Larbalestier, H. W. Weijers *et al.*, IEEE Trans. Appl. Supercond. **22**, 4300704 (2012).